Global and Planetary Change 193 (2020) 103265

Contents lists available at ScienceDirect

Global and Planetary Change

journal homepage: www.elsevier.com/locate/gloplacha

Sea surface temperature variability in the Arctic Ocean and its marginal seas in a changing climate: Patterns and mechanisms

K.S. Carvalho, S. Wang*

Department of Land Surveying and Geo-Informatics, The Hong Kong Polytechnic University, Hong Kong, China

ARTICLE INFO

Keywords:
Sea surface temperature
Arctic Ocean
Climatic variables
Correlation

ABSTRACT

Understanding temporal variability of sea surface temperature (SST) patterns plays a crucial role in providing insights into the mechanisms causing extreme weather and climate events as well as oceanic and atmospheric teleconnections. This study presents an in-depth analysis of the SST patterns of the Arctic Ocean and its marginal seas on interannual and seasonal timescales from 1982 to 2018. The results reveal potential relationships between SST and climatic variables in order to improve our understanding of underlying physical mechanisms influencing the SST variations in a changing climate. Our findings disclose that the Arctic Ocean shows an overall warming trend, and the Nordic Seas have the highest SST compared to its neighboring seas. The Barents Sea shows spatially varying seasonal trends due to ice cover changes and warm water circulation within the Nordic Seas. Correlation analysis was also performed to facilitate further understanding of climate-induced SST changes. It reveals that climate variables interact differently with the Arctic Ocean SST on a regional scale and vary with different degrees of influence. Notable relationships between SST and climate variables improve understanding of differing trends on spatial and temporal scales. In addition, the wavelet coherence speculates that a significant in-phase relationship exists between SST and Greenland Blocking Index (GBI), which facilitates further studies exploring the complex mechanisms causing teleconnection patterns related to the Arctic Ocean.

1. Introduction

The global average sea surface temperatures (SSTs) have been increasing since the beginning of the 20th century, where the rates of increase are higher near the surface of the ocean (greater than 0.1 °C per decade in the upper 75 m) (IPCC, 2014). This key factor helps in understanding the air-sea interaction and its role in global climate studies (Tang, 2012). The ocean's thermal inertia that translates to SST is communicated to the atmosphere via air-sea fluxes and the exchange of energy (Deser et al., 2010a). The global oceans are known to be taking up at least 90% of the heat present in the atmosphere, which has affected the ocean temperature and currents (Zanna et al., 2019).

Climate change in the Arctic and subarctic have been highlighted in global warming impacts. The Arctic Ocean and adjacent land masses are experiencing intense climate change. As evidenced by paleo (Miller et al., 2010) and observational data (Serreze et al., 2009), the temperature changes in these regions are 3–4 times greater than the average for the Northern Hemisphere, and is termed as the Arctic amplification (Manabe and Stouffer, 1980; Simmonds, 2015). This phenomenon "amplifies" or makes the Arctic climate change driven by any global radiative forcing greater than in other climate zones, and is caused by the ice-albedo feedback mechanisms, atmospheric and ocean heat advection, as well as changes in water vapor (Serreze and Serreze and Barry, 2011; Lee et al., 2017). Arctic Ocean SST is strongly influenced by sea ice and related melt water, brine rejection, continental runoff and upward heat fluxes from the deeper warm ocean (Stroh et al., 2015). A number of studies on the SST warming have been conducted in the recent decades. Comiso (2003) used the thermal infrared data from the Advanced Very High Resolution Radiometer (AVHRR) sensor carried on-board the National Oceanic and Atmospheric Administration (NOAA) satellites, and concluded an increasing SST trend for the period of 1981–2001. Chepurin and Carton (2012) used the Pathfinder SST data and operational SST products from NOAA and UK Meteorological Office to investigate connections between Arctic SST variations and sub polar gyres in the "Atlantic" sector and further north of the Arctic Ocean.

SST has been one of the most important measured variables of the ocean which affects the climate system and has attracted much scientific attention (Reynolds et al., 2007; Deser et al., 2010a; Carvalho and Wang, 2019). In the recent past, Arctic amplification and consequent warming have been studied using climate models, and are proved to be a result of anthropogenic global warming (Holland and Bitz, 2003). The

* Corresponding author.
E-mail address: shuo.s.wang@polyu.edu.hk (S. Wang).

https://doi.org/10.1016/j.gloplacha.2020.103265
Received 21 April 2020; Received in revised form 18 June 2020; Accepted 29 June 2020
Available online 08 July 2020

Arctic Ocean warming caused by ice-albedo effects and atmosphere-ocean dynamics have also been studied to identify relationships with climate change (Deser et al., 2010; Chepurin and Carton, 2012; Steele and Dickinson, 2016). In order to improve knowledge of climate change impacts on the Arctic Ocean SST, it is desired to derive a comprehensive outlook on the SST variability in the Arctic Ocean and to compare the trends between its marginal seas. In addition, previous studies have indicated that the ice-albedo feedbacks and heat fluxes have been closely associated with the Arctic Ocean. It is necessary to further explore the atmosphere-ocean interactions by analyzing various variables such as air temperature, water vapor, wind speed, and total cloud cover on different spatial and temporal scales.

Specifically, this study aims to analyze the spatial and temporally varying SSTs of the Arctic Ocean and its marginal seas, as well as to reveal relationships between SST and climatic variables including air temperature (T2m), total column water vapor, wind speed, total cloud cover (TCC), ozone, sea level pressure (SLP), and sea ice concentration (SIC). This will help characterize the dynamics of SST and deduce the local covariance between SST and climatic variables. Furthermore, the relationships, trends and periodicities between the Arctic SST and the Greenland Blocking Index (GBI) will be uncovered to reveal the influence of teleconnections on the Arctic Ocean SSTs. The NOAA Optimum Interpolation SST dataset will be used to reveal the spatiotemporal variability of the Arctic Ocean SST in a global warming perspective for the period from January 1982 to December 2018.

This paper will be organized as follows. Section 2 will introduce data sources and methods. Section 3 will present a thorough analysis on spatial and temporal distributions of the Arctic Ocean SST and its correlations with climatic variables and GBI. Section 4 will provide a detailed and in-depth discussion on the Arctic Ocean SST characteristics and underlying mechanisms causing the SST variability, as well as potential linkages between ocean temperatures and regional climate indices. Finally, Section 5 will provide conclusions and main findings of this study.

2. Data and methods

2.1. Data sources

To analyze the SST characteristics of the Arctic Ocean and its marginal seas (as shown in Fig. 1), the NOAA Optimum Interpolation SST (OI SST Version 2) dataset was used for the period from January 1982 to December 2018, and was obtained from the NOAA/Oceanic and Atmospheric Research/Earth Science Research Laboratory/Physical Sciences Division (NOAA/OAR/ESRL/PSD), Boulder, Colorado, USA (http://www.esrl.noaa.gov/psd/). The analyses were designed by combining multiple observations from different platforms (satellites/ships/buoys) on a complete regular grid. The dataset has undergone bias adjustments of satellite and ship observations to compensate for platform differences and sensor biases (Reynolds et al., 2007). The dataset contains monthly SST fields derived by averaging daily values for each month. The analysis uses satellite SST values and simulated SSTs using sea ice cover data. This improved analysis is independent of satellite biases (Reynolds and Marsico, 1993). The dataset has been regridded to a spatial resolution 0.25°, which was used to examine the variability in SSTs. Sea ice data is also sourced from the same dataset and is recorded as monthly sea ice concentration values.

The gridded data from 1982 to 2018 for surface level meteorological parameters and air-sea heat fluxes (0.25° × 0.25° spatial grid) were extracted from the ERA-Interim full resolution database (https://www.ecmwf.int/). The ERA-Interim project serves as a fundamental improvement in stratospheric properties, hydrological cycles and effective timely records of climate parameters (Dee et al., 2011; Wang et al., 2018; Wang and Wang, 2019; Zhang et al., 2019; Chen et al., 2020). These data were correlated with the SST data to investigate the effects on the SST variability. In addition, GBI data were downloaded from the

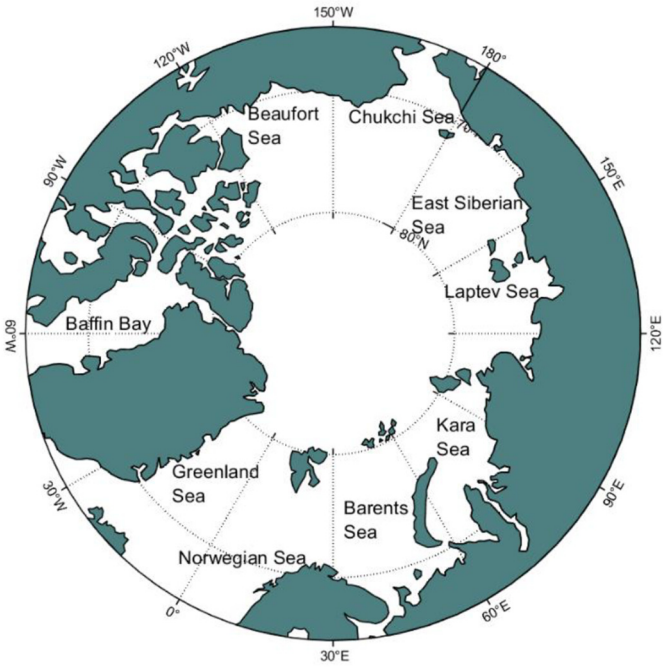

Fig. 1. Map of the Arctic Ocean and the marginal seas.

NOAA Climate Prediction Center (https://www.cpc.ncep.noaa.gov/). GBI is defined as the mean 500 hPa geopotential height for the 60–80°N and 20–80°W region in the Northern Hemisphere (Hanna et al., 2016). Cross-wavelet analysis was used to analyze the time series and space-time relationships with the Arctic Ocean SST for the period of 1982–2018. The spatial and temporal distribution of SST data obtained from NOAA was used to study interannual and seasonal variability on a geographical scale. Annual and seasonal SST trends were calculated for each grid and for the entire study area. Linear trends were calculated on the basis of least squares method using the climate data toolbox developed by Greene et al. (2019). The mentioned toolbox contains various mathematical functions that can be used in Earth sciences and climate change studies. Seasons are defined as Winter (December–January-February), Spring (March–April-May), Summer (June–July-August) and Autumn (September–October-November). In order to study the interannual variability, the dataset was first detrended and then a measure of standard deviation was calculated. The monthly effects of climate parameters on the Arctic Ocean SST were tested using the correlation coefficient (R) at 95% confidence levels. To identify significant correlation ranges, a *p*-value of 0.05 was used as the significance level. Spatial correlation coefficients with *p*-values less than 0.05 are considered statistically significant (Fisher, 1992).

2.2. Wavelet analyses

The techniques of wavelet analysis have become gradually popular with time series examinations. Here, we use the Matlab software package developed by Grinsted et al. (2004) to perform wavelet coherence and cross wavelet analysis, and apply the wavelet methodology adopted by Torrence and Compo (1998) to analyze the time-frequency relationship between Arctic Ocean SST and GBI. Wavelet transforms (CWT) expand time series into time frequency domains and can be studied for trends and local intermittent periodicities. Wavelets are characterized by how localized it is in time (Δt) and frequency ($\Delta\omega$) or bandwidth (Grinsted et al., 2004). The Morlet wavelet ($\omega = 6$) is an appropriate choice providing a good balance between time and frequency localization. The CWT of a time series d with respect to the wavelet ψ is defined as

$$W_{d,\psi}(s,t) = (d(t) * \psi_s(t)) \quad (1)$$

where t is time, ψ is the wavelet and s is the scale (which is linearly related to the characteristic period of the wavelet). The wavelet power is defined as $|W_{d,\psi}|^2$. Wavelet transforms are affected by edge artifacts due to time bounds in data $d(t)$, and hence a Cone of Influence (COI) is introduced so that edge effects can be ignored (Torrence and Compo, 1998). The COI is the area in which a wavelet power caused by a discontinuity at the edge is dropped to e^{-2} of the value at the edge.

The cross wavelet transform (XWT) of two time series x_n and y_n is defined as $W^{XY} = W^X W^{Y*}$, where * indicates complex conjugation. Furthermore, the cross wavelet power is defined as $|W^{XY}|$. As defined by Torrence and Compo (1998), the theoretical distribution of two time series with background power spectra ${P_k}^X$ and ${P_k}^Y$ is given as

$$D\left(\frac{|W_n^X(s) W_n^Y * (s)|}{\sigma_X \sigma_Y} < p\right) = \frac{Zv(p)}{v} \sqrt{P_k^X P_k^Y} \quad (2)$$

where $Zv(p)$ is the confidence level associated with probability p for a probability density function (pdf) defined by the square root of the product of two χ^2 distributions. To assess the phase difference between the two different time series, the mean and confidence interval of the phase difference are estimated. The circular mean set of angles (a_i, $i = 1 \ldots n$) is given by (Zar, 1999):

$$a_m = \arg(X, Y) \text{ with } X = \sum_{i=1}^{n} \cos(a_i) \text{ and } Y = \sum_{i=1}^{n} \sin(a_i), \quad (3)$$

The cross wavelet phase angle is calculated as a scatter of the angles around the mean. Hence, the circular standard deviation is defined as:

$$s = \sqrt{-2 \ln\left(R/n\right)}, \quad (4)$$

where $R = \sqrt{X^2 + Y^2}$.

The circular standard deviation is analogous to linear standard deviation and varies from zero to infinity. Another useful measurement in wavelet analysis is to understand the degree of coherency of the CWT in time and space. Torrence and Webster (1999) define wavelet coherence of two time series as:

$$R_n^2(s) = \frac{|S(s^{-1} W_n^{XY}(s))|^2}{S(s^{-1} |W_n^X(s)|^2) . S(s^{-1} |W_n^Y(s)|^2)}, \quad (5)$$

where S is a smoothing operator. The smoothing operator can also be defined as:

$$S(W) = S_{scale}(S_{time}(W_n(s))), \quad (6)$$

where S_{scale} denotes smoothing along the wavelet scale axis and S_{time} is smoothing in time.

The histograms (pdfs) of both time series were checked to observe for normality. Both time series have near normal distributions and hence were not converted into log or percentile scales. This is an essential step in statistical analysis of time series. CWTs of geophysical time series that are far from normal produce unreliable and non-significant results (Grinsted et al., 2004). From the two CWTs, the XWT is calculated which determines regions of high common power and phase relationships between two time series (Grinsted et al., 2004).

3. Results

3.1. Spatial and temporal distribution of Arctic Ocean SST

The Arctic Ocean SST and seasonal means are used to characterize the dynamics of SST. The annual average SST of the Arctic Ocean is 1.32 ± 1.5 °C (Fig. 2a). The hottest areas of 6 °C and above cover 3.5% of the Arctic Ocean, most of which is present in the Norwegian Sea. As shown in Fig. 2, the Chukchi Sea has an average SST of 0.86 °C. Relatively higher temperatures of 4–7 °C and − 1 − 5 °C are noticed in the Nordic Seas (Norwegian Sea and Greenland Sea respectively) and the Barents Sea shows values between 0.2 and 3 °C. Here, the Nordic Seas were defined according to Furevik et al. (2007). Most of the Arctic Ocean that borders Russia and Canada are of low temperatures. As it goes poleward from 78°N, smaller positive values of < 1 °C are seen. This connects well with the studies carried out by Serreze et al. (2009) for the study period of 2003–2007. In the given time period, the annual trend distribution varies locally in the seas belonging to the Arctic Ocean (Fig. 2b). The Arctic Ocean shows an overall warming trend of 0.036 ± 0.03 °C/year. The Barents Sea has a wide trend (spatially) and is −0.01 − 0.05 °C/year. Similarly, Greenland Sea shows a wider range of trends between −0.03 and 0.02 °C/year is noticed and varies spatially. The Norwegian Sea has a warming trend of 0.04–0.07 °C/year. All other marginal seas show relatively weak warming trends (−0.01–0.01 °C/year). To supplement further analysis in terms of magnitude, the decadal SST means (Fig. 2c) show similar spatial patterns as the annual means, where the Norwegian Sea has the highest values ranging from 6.5 to 8.2 °C. The Chukchi Sea shows decadal mean values of −0.8–2 °C in contrast to the annual mean ranging between −0.5 and 0.2 °C. The decadal trends also vary spatially; Barents Sea values range between a weak cooling trend of −0.02 and a warming trend of 1.04 °C/decade. The Chukchi Sea shows a lower decadal trend (as compared to annual trends) ranging from 0.01 to 0.04 °C/decade, indicating weak warming signals. In addition, standard deviation of Arctic Ocean SST is approximately 0.1–0.2 °C in the Chukchi Sea (Fig. 3). Barents Sea and Greenland Sea show a standard deviation of 0.4–0.7 °C and 0.2–0.8 °C, respectively. This indicates high variability where these seas warm up greatly in the summer and cool (freeze) in the winter. Marginal seas of East Siberian and Laptev Seas show low standard deviations of less than 0.12 °C.

The spatiotemporal distribution of mean winter SST is similar to the annual mean SST for the Arctic Ocean in the Nordic Seas which is between 0.4 and 2 °C for Greenland Sea and 4.5–6.4 °C in the Norwegian Sea which is the highest. The Barents Sea shows an average weak mean SST of 0.8 °C while the values of its western region range from 1 and 1.6 °C (Fig. 4). The relatively highest temperatures (greater than 6 °C) covers 2.8% of the Arctic Ocean. Colder areas of 0–1 °C cover more than 80% of the study area, notably the Beaufort, East Siberian and Laptev Seas. The winter SST trend is highest in the Norwegian Sea and Barents Sea at 0.03–0.05 °C/year; typical regions are off the coasts of Scandinavia and northwestern Russia that show higher values of 0.07 °C/year. The Greenland Sea has a unique overall winter trend of −0.2 to 0.02 °C/ year on a spatial scale, thereby showing warming and cooling trends with time in different parts of the sea. Mean spring SST is found to have a similar spatiotemporal variation as the winter mean SST where the Greenland Sea shows a spatially varying trend and the other Nordic Seas have the highest trend.

The spatiotemporal distribution of mean summer temperature shows a high of 7–11 °C in the Norwegian Sea and followed by 4–7 °C in the Barents Sea and 2–5 °C in Greenland Sea. This exemplifies previous findings where the Nordic Seas are found to have maximum summer SST means (Chepurin and Carton, 2012). Chukchi Sea summer SSTs are higher than preceding seasons at 2.4–4 °C. Compared to winter and spring mean SSTs, Baffin Bay (west of Greenland) shows relatively higher SST means in the summer calculated at 3 °C unlike the preceding seasons of 0–0.5 °C. The same is observed for Kara Sea, Laptev Sea and the East Siberian Sea which are relatively warmer than previous seasons. The Beaufort Sea has a mean SST of 2 °C in the summer whereas the mean SST in other seasons is below 1 °C. Cooling summer trends can be seen in the Laptev Sea (off the coast of Sakha Republic in Russia). It should be noted that while the northern Barents Sea shows a relative cooling trend of −0.03 °C/year, the southern parts show a warming trend, particularly near the coasts. The cooling summer trend in the Barents Sea can be due to oceanographic properties (e.g., salinity, density, and depth). Salinity variations on a spatial scale can also be considered a primary factor in SST variability. Brine rejection which is a

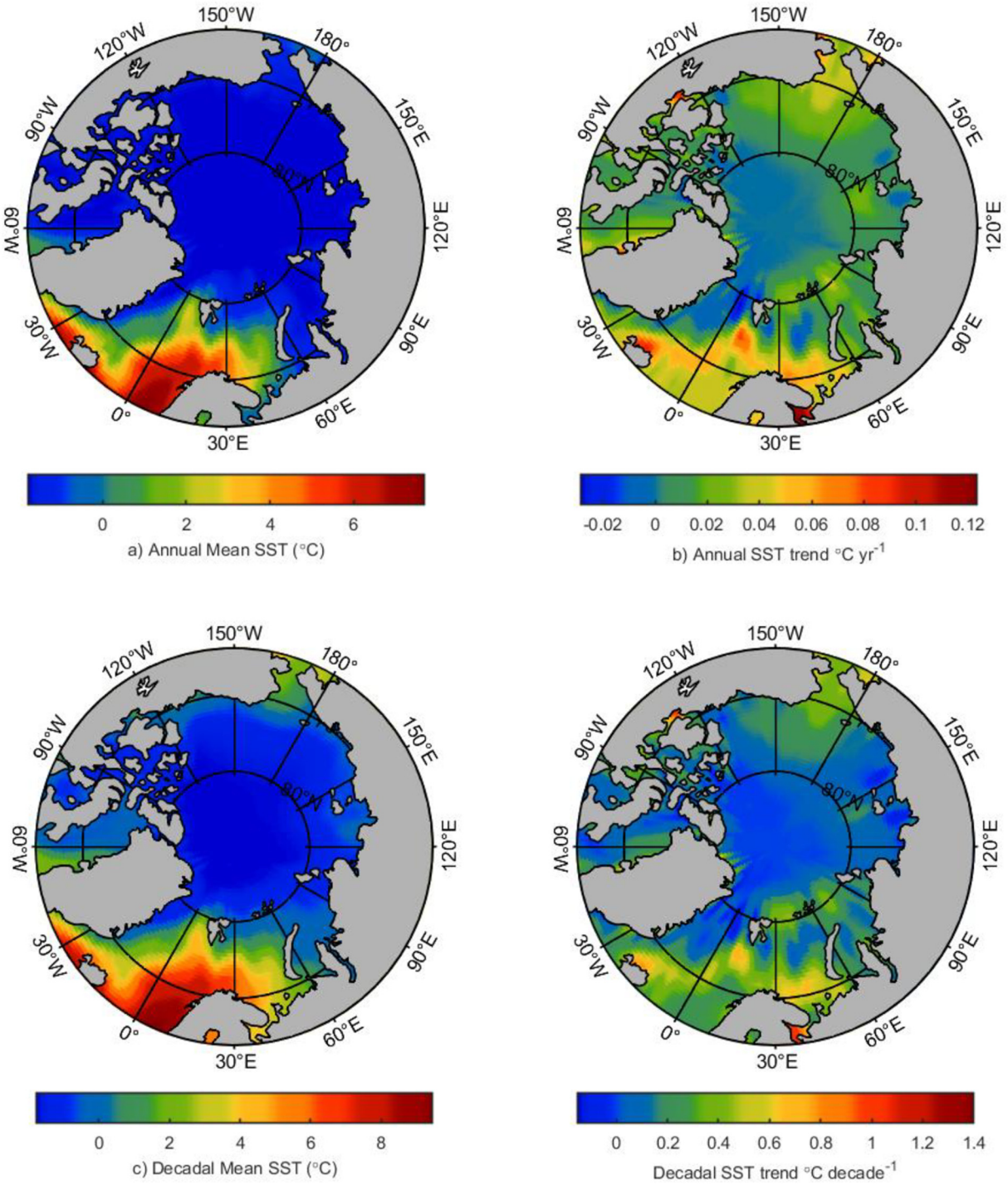

Fig. 2. Spatiotemporal distribution of a) Annual Mean SST b) Annual SST trends c) Decadal Mean SST and d) Decadal SST trends for the period 1982–2018. The maps represent annually/decadal averaged means and trends.

phenomenon in colder waters may cause comparatively colder trends in certain parts of the Barents Sea; Stroh et al. (2015) mentioned in their paper of brine rejection being an agent of Arctic Ocean SST changes. The northern region has seen a relative sea ice decrease in the past decades coupled with reduced sea-surface albedo. Spatial variations in the summer trends in the Barents Sea are due to sea ice extent being comparatively higher near Novaya Zemlya (north) than the rest of the sea (Jakowczyk and Stramska, 2014). The comparatively higher coastal trends (warming) can be ascribed to increased freshwater run-off from the nearby coastal land. This is because the ice extent does not play a significant role in summer SSTs (Pavlova et al., 2014). All other regions show notable warming summer trends. Mean autumn SST shows similar spatiotemporal characteristics as the previous season (summer); the only difference is Laptev Sea that shows a decreased mean at 1 °C. Most of the Arctic Ocean show uniform warming Autumn trends. The Barents Sea shows a warming trend (Kola Peninsula and Kolguyev Island) and a cooling trend further north (near Novaya Zemlya (Russia)). This is also attributed to spatial changes in sea ice due to the refreeze season in autumn. This conclusion is based on the inverse relationship between SST and SIC in the northern Barents Sea (Fig. 6g). Greenland Sea has an autumn warming trend of 0.02 °C/year, and the Chukchi Sea has a slightly higher trend of 0.04 °C/year. Fig. 5 and Table 1 summarize

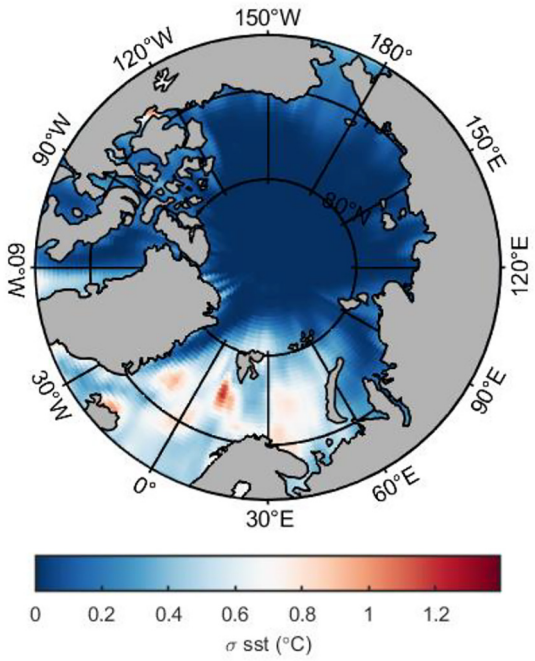

Fig. 3. Spatiotemporal distribution of standard deviation of Arctic Ocean SST.

interannual and seasonal statistics of the Arctic Ocean SSTs.

3.2. Correlation between Arctic Ocean SST and atmospheric variables

There is a highly positive correlation ($R > 0.75$) between SST and air temperature (T2m) over more than 70% of the study area, indicating that air temperature has a noticeable effect on the SST of the Arctic Ocean (Fig. 6a). As it goes poleward from 75°N, the positive correlation is ambiguous due to ice cover. And Laptev and Kara Seas have a comparatively lower positive correlation of 0.6 as compared to other marginal seas of the Arctic Ocean. In addition, a significant correlation exists between SST and water vapor over 81% of the study area (Fig. 6b). The relatively high correlations ($R > 0.7$) are found in the Nordic Seas, Kara Sea, Chukchi Sea and Beaufort Sea. The high correlation between SST and water vapor can cause an increase in surface air temperatures as well (Fig. 6a and b), thereby proving a strong link between the three variables. Such an interactive system coupled with increase in downward infrared radiation has also been hinted as one of the underlying causes of the Arctic warming (Lee et al., 2017; Luo et al., 2017; Yao et al., 2017). A phenomenon of "moisture intrusions" which has been met with great attention, can also be attributed to increases in Arctic temperatures (Screen et al., 2018). A strong relationship between SST, air temperature and water vapor can thereby affect atmospheric circulation patterns and fuel polar cyclones as an additional consequence. A significant negative correlation between SST and Ozone ($R < -0.4$) is found over 65% of the Arctic Ocean (Fig. 6c). In comparison, the Chukchi Sea has a higher negative correlation ($R < -0.7$), indicating that the decrease in ozone greatly affects (and increases) the Arctic Ocean SST in the Chukchi region. Other seas such as Greenland Sea, Barents Sea and Chukchi Sea show the R values between -0.5 and -0.3.

The spatial distribution of correlation coefficients between SST and wind speed shows a wide range from -0.6 to 0.4 (Fig. 6d). It can be seen that a significant correlation exists over 52% of the entire study area. Specifically, a high negative correlation ($R < -0.5$) between SST and wind speed is found in Norwegian Sea. This is due to the fact that the relationship between SST and wind speed tends to be negative in general (Hurrell, 1995). The theory behind this is that the increasing wind speed would tend to lower the SST by breaking down the

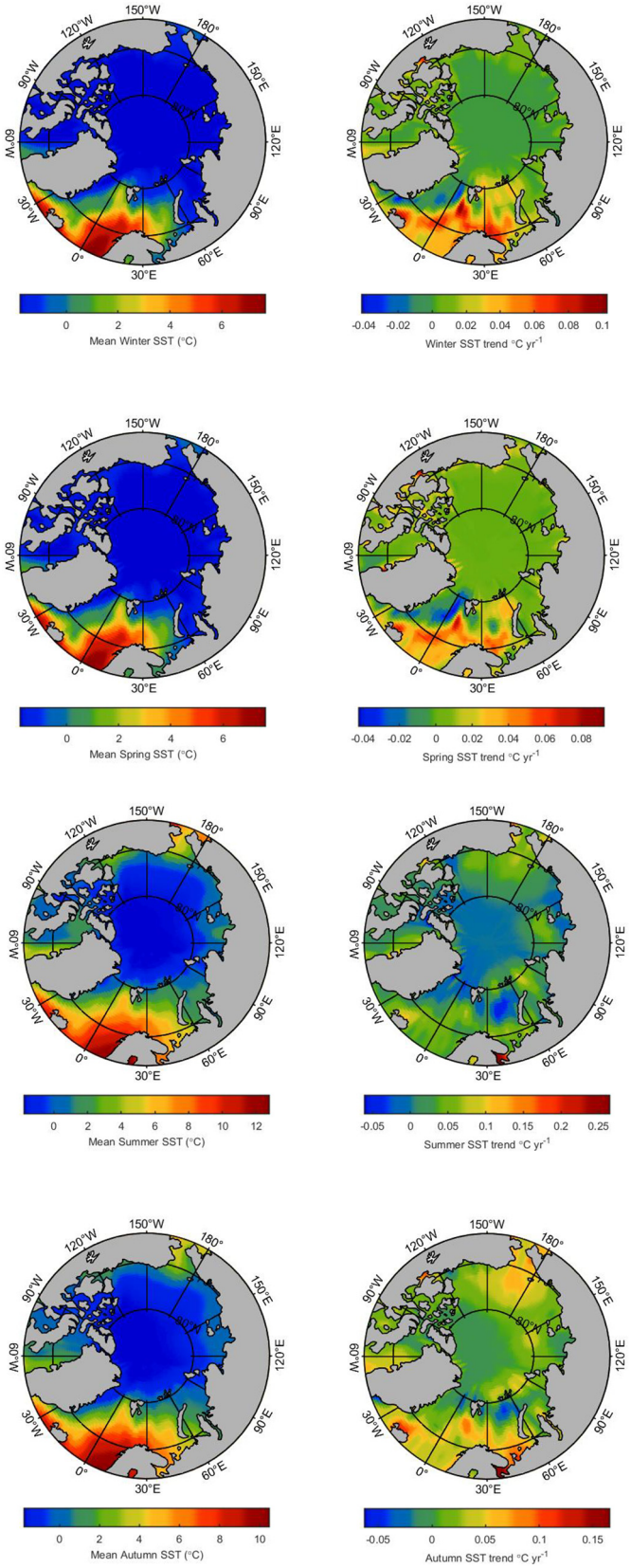

Fig. 4. Spatiotemporal distribution of mean seasonal SST and seasonal SST trends. Regions in red indicate highest means and trends while blue indicates relatively colder means and trends. (For interpretation of the references to colour in this figure legend, the reader is referred to the web version of this article.)

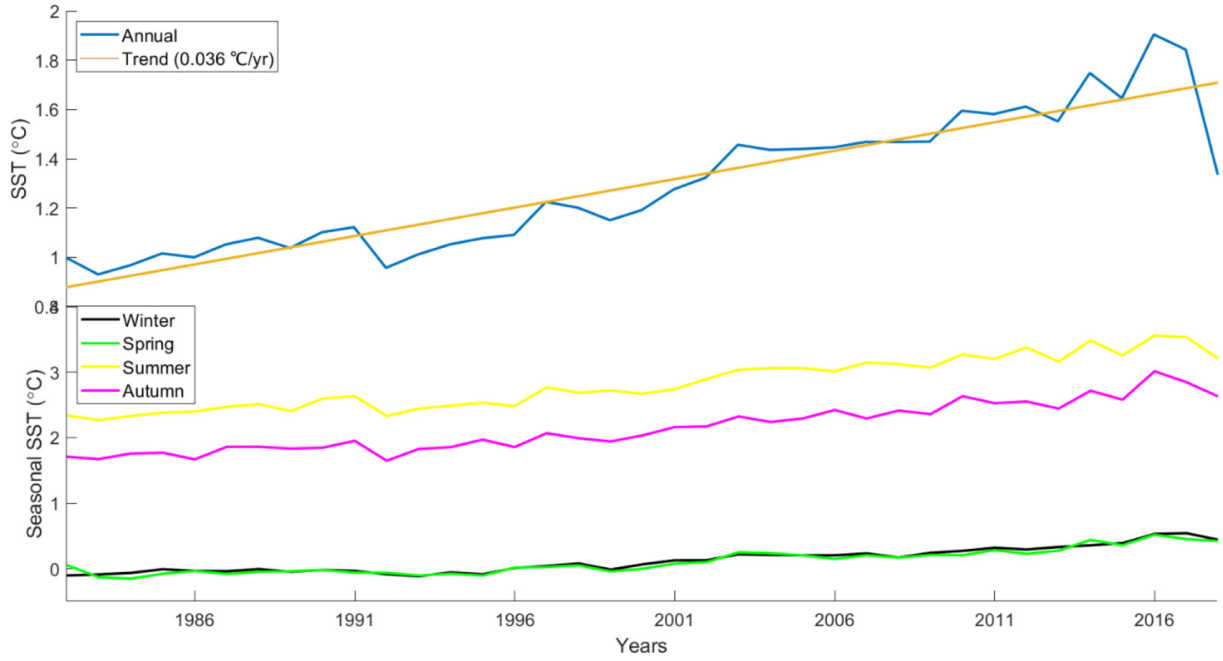

Fig. 5. The interannual and seasonal SST of the Arctic Ocean. (Top) The yellow line shows a linear trend in SST of 0.036 ℃/year (Regression Statistics: $R^2 = 0.85$; Equation: $y = 0.023\times + 0.855$). (For interpretation of the references to colour in this figure legend, the reader is referred to the web version of this article.)

Table 1
The Arctic Ocean SST characteristics on different temporal scales.

Statistics	Interannual SST characteristics	Seasonal SST characteristics			
		Winter	Spring	Summer	Autumn
Mean (°C)	1.302 ± 1.44	0.12 ± 0.18	0.11 ± 0.17	2.82 ± 0.39	2.15 ± 0.36
Trend (°C/yr)	0.036	0.016	0.015	0.034	0.032
Max SST (°C)	1.904	0.54	0.518	3.556	3.012
Min SST (°C)	0.930	−0.116	−0.152	2.268	1.647

stratification of the surface water, thereby leading to the upwelling of colder water to the subsurface. All other marginal seas have low to negligible relationships between SST and wind speed. The Arctic Ocean shows a negligible correlation between SST and SLP (Fig. 6e). However, there is a small negative correlation ($R < -0.4$) between SST and SLP over northern Chukchi Sea and Beaufort Sea. Approximately 42% of the study area shows a significant correlation between SST and TCC. And a low negative correlation ($R = -0.2$) between SST and TCC exists in Barents Sea, Kara Sea and Beaufort Sea (Fig. 6f). This suggests that TCC changes do not greatly affect the variations in SST. A positive correlation ($R = 0.5$) between SST and TCC is found in parts of Baffin Bay (off the western coast of Greenland).

There is a significant negative correlation between SST and SIC over 89% of the study area (Fig. 6g). This can be connected to the polar amplification in the northern hemisphere (Holland and Bitz, 2003). Decreasing sea ice concentration exposes much of the oceans to sunlight and oceans, having a lower albedo, absorb more of the incoming solar radiation. This can lead to more ice melting and the chain goes on, which is commonly referred to as the sea-ice albedo effect. Besides the spatiotemporal relationships between these two variables, there is no significant relationship between the Greenland and Norwegian Seas. It should be noted that sea ice concentration simulations using climate models are ice free in these regions (Chepurin and Carton, 2012), and hence its relationship with SST is impossible to comprehend.

3.3. Cross wavelet and coherence analysis

The CWT for the Arctic Ocean SST has stable periodic characteristics (see the horizontal band) with high power oscillations in the 9- to 15-month period band throughout the study period. This can imply a considerable power spread in the yearly (12 month) bands (Fig. 7). High power oscillations are scattered in the CWT plot for GBI (Fig. 8). However, significant peaks are noticed in the months from 2008 to 2014 in the 12-month and 36-month bands.

In the XWT plot (Fig. 9), there are considerable links between GBI and the Arctic Ocean SST in regions indicated by black contours. Common power is seen in the 12-month band where the GBI and SST have an in-phase relationship and SST is leading in the period of 2006–2015. Similarly, a positive correlation is also seen in the period of 1988–1994, which infers that an increase in GBI causes an increase in the Arctic Ocean SST (positive correlation). On the contrary, regions outside the areas of significant power show a chaotic relationship between SST and GBI, and thus phase relationships cannot be easily deciphered in these regions. The XWT average phase angle for significant regions is 19.48 ± 3.6 (where 3.6 is the circular standard deviation). The XWT helps to understand the phase spectrum. The WTC plot (Fig. 10) can be used to decipher frequency bands and time intervals in which the two different time series co-vary. In the WTC, significant correlations can be seen in the periods of 1988–1994 and 2012–2014 in the 12-month period; in the second period the Arctic Ocean is found to lead GBI. Another interesting inference is the positive correlation in the 60-month period band from 1988 to 1993, where the Arctic Ocean SST leads GBI. Wavelets are unique which can differentiate between different relationships occurring at the same time but at different frequencies.

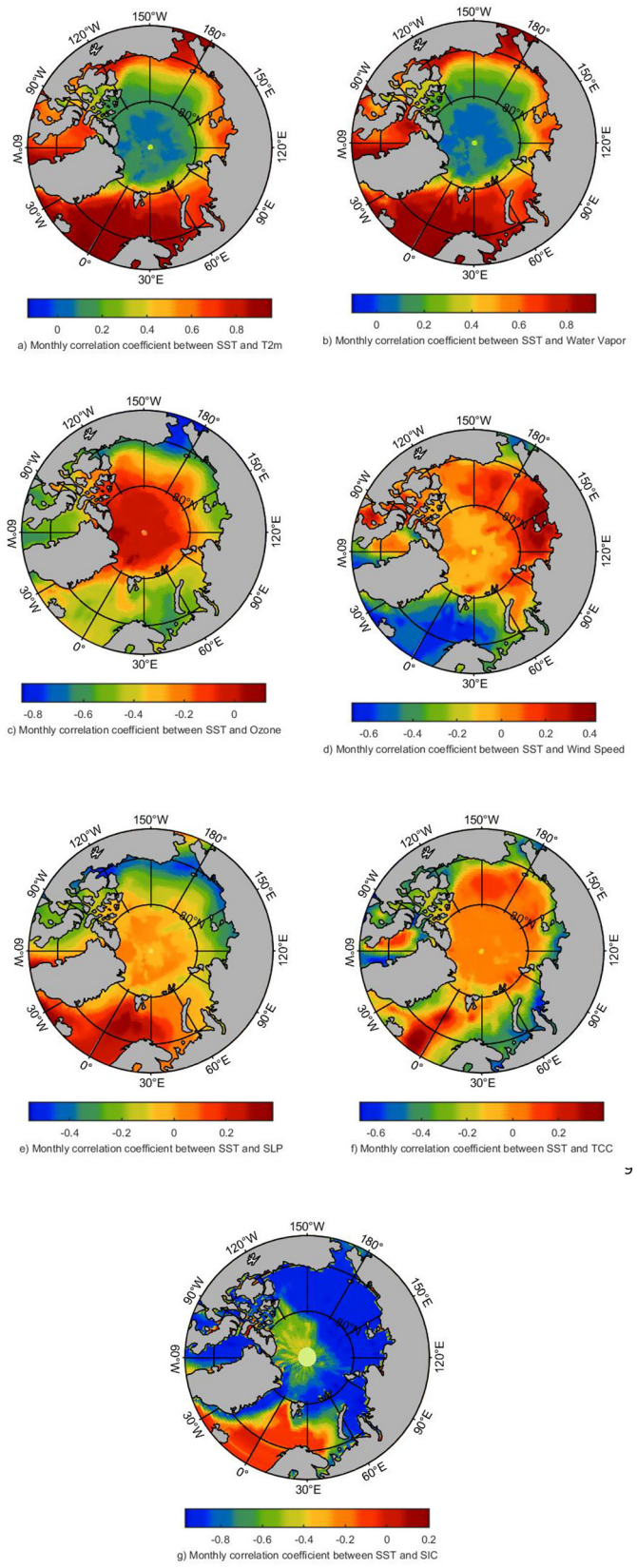

Fig. 6. Monthly correlation coefficients (R) between Arctic Ocean SST and climate variables. A value of −1 indicates a strong negative correlation while +1 indicates a strong positive correlation (0 indicates no correlation). The area of significance (as explained in text) is based on those regions where the associated *p*-value ≤.05 (where α = 0.05 at the 5% significance levels).

4. Discussion

4.1. Arctic Ocean SST characteristics

The Arctic Ocean SST characteristics were analyzed on spatial and temporal scales. The maximum SST for the Arctic Ocean was recorded at 1.9 °C as compared to the mean of 1.3 °C in the year 2016; in the same year, spring, summer and autumn seasons also experienced maximum temperatures. From a global warming perspective, these results postulate that 2016 was the hottest year for the Arctic Ocean. And the winter SST was highest in 2017. Colder years existed in the 1980s and early 1990s, which implies that SSTs have increased since the 20th century and the recent past has been characterized by relatively high SSTs. It is worth mentioning that increasing SSTs can have significant effects on heat storage feedbacks and the Arctic cryosphere in general (Overland et al., 2019).

It can be seen that the Nordic Seas and the Chukchi Sea are characterized by high SST means and trend variations. The seas of the Arctic Ocean such as the Greenland Sea, Norwegian Sea, Barents and Chukchi Sea show particularly high temperature means and trends for the period from January 1982 to December 2018. This can be attributed to the advection of warm water from the North Atlantic (affecting Greenland Sea, Norwegian Sea and Barents Sea) and North Pacific Oceans (affecting Chukchi Sea) by their respective currents. Intrusion of warmer waters and consequently, ocean heat has impacted the marginal seas of the Arctic. This ocean heat transport is responsible for variations in Arctic Ocean temperatures and sea-ice variability, two closely linked variables whose effects have been exemplified in the Barents Sea (Årthun et al., 2019; Wang et al., 2019). The Greenland Sea shows a comparatively smaller SST means and variations. This can be explained by the flow of cold polar waters from the Arctic towards lower latitudes via the Fram Strait, and is characterized by the East Greenland Current (EGC). The EGC flows along the eastern coast of Greenland and enters the Atlantic Ocean via the Fram Strait (Furevik, 2000). In the southern Greenland Sea near Iceland, the SST values are higher than further north. This can be a most likely case of air-sea interactions off the coast of Iceland that dominates the SST (Fig. 6a). This conclusion is arrived at since the correlation between SST and air temperatures are found to increase southward along the coast of Greenland (from 0.4 to 0.8).

The Norwegian Sea in particular is found to have the highest mean SST of 4–7 °C and an interannual warming trend of 0.04–0.07 °C/year. Such a relatively high warming trend is due to these regions being ice-free, thereby allowing more absorption of incoming solar radiation. A theory revolving around the involvement of thermal forcing of the North Atlantic Oscillation (NAO) in the evolution of SSTs in the Nordic seas can be a cause of comparatively higher SSTs in the Norwegian Sea (Flatau et al., 2003). In addition, the Arctic Ocean SST warming trends are higher in summer (0.036 °C/year) as compared to all other seasons (with autumn trends at 0.032 °C/year). This relatively high summer warming trend when sea ice concentration is low, can be a result of highly amplified summer feedbacks.

The spatiotemporal structure of seasonal SST highlights that the Norwegian Sea is characterized by highest mean seasonal SST (in all four seasons). This is followed by the Greenland Sea and Barents Sea which shows higher SST as compared to most parts of the Arctic Ocean. One particular sea of interest is the Chukchi Sea which shows considerable SST variations across four seasons. The Chukchi Sea exhibits high mean values in the summer at 2.4–4 °C as compared to 2.2–3.7 °C in autumn and 0–0.5 °C in the winter and spring. This drastic change in SST on a seasonal basis can be linked with ocean advection dynamics and the air-sea interactions in the Northern Pacific Ocean (Yeo et al., 2014; Steele and Dickinson, 2016). Throughout all seasons, the Greenland Sea has approximately similar mean SST of 2.5 °C. And the Norwegian Sea and Barents Sea show high warming trends in winter and spring. However, the spatial distribution drastically changes in summer; the Norwegian Sea has an SST of 0.05–0.1 °C/year while

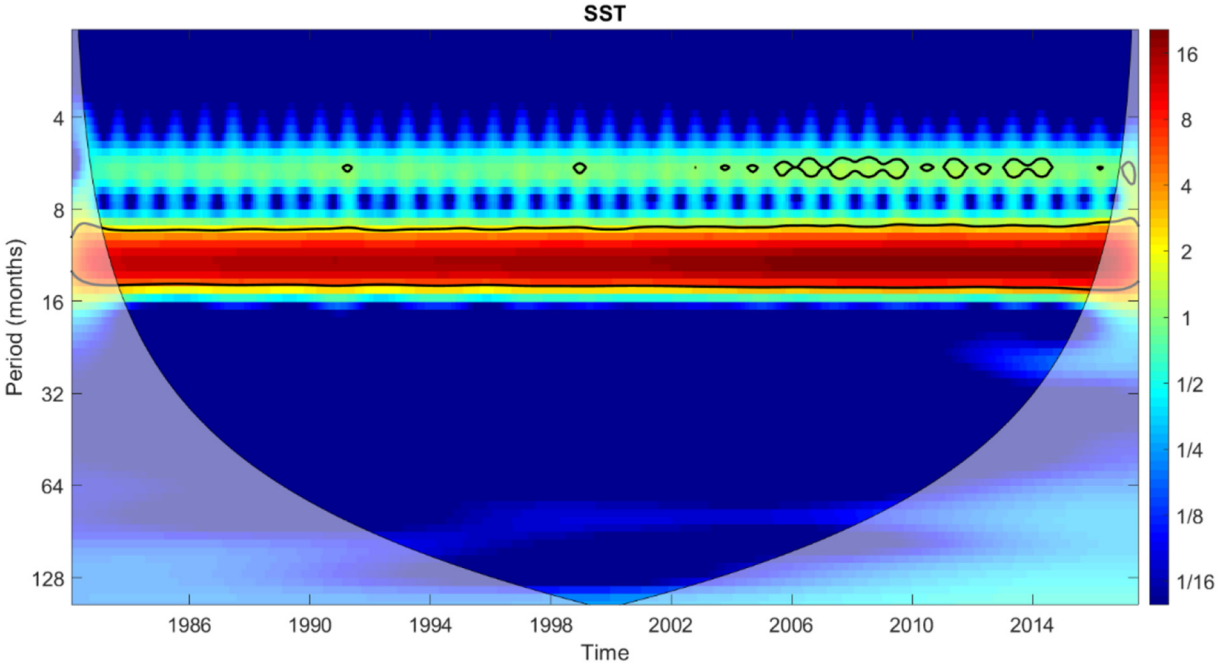

Fig. 7. The Continuous Wavelet Spectrum (CWT) for the Arctic Ocean SST. Thick black contours designate the 5% significance levels against red noise and the cone of influence (COI) where edge effects may distort the analysis as shown in a lighter shade. (For interpretation of the references to colour in this figure legend, the reader is referred to the web version of this article.)

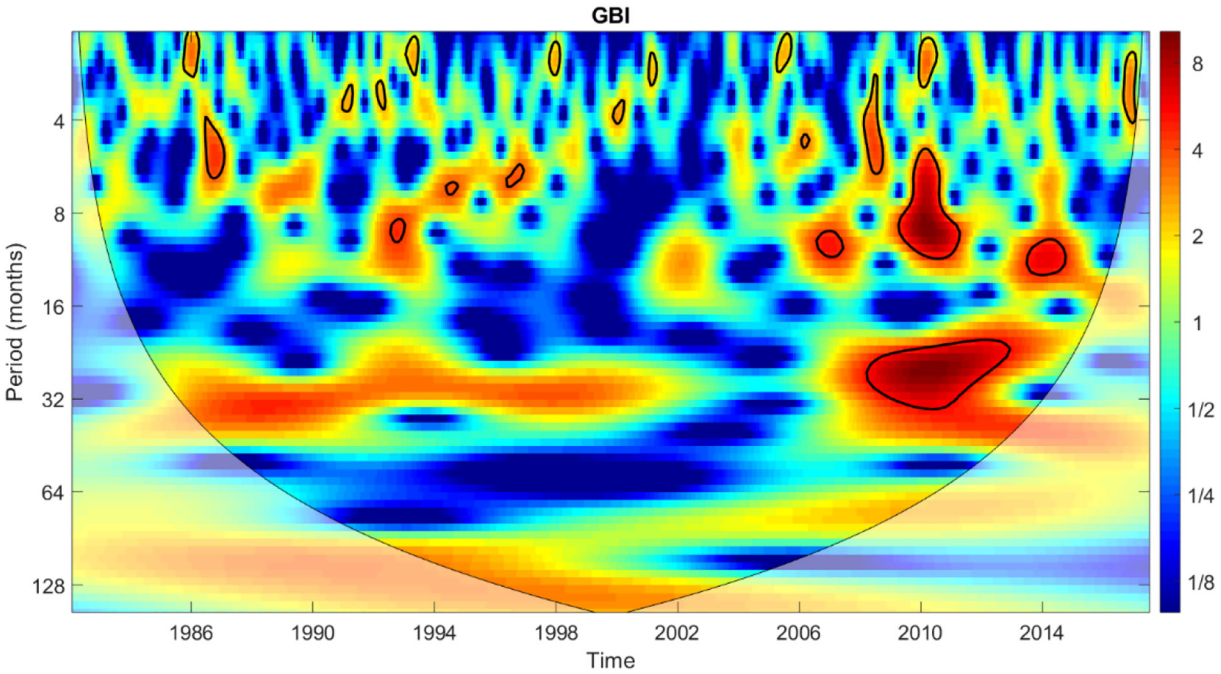

Fig. 8. The Continuous Wavelet Spectrum (CWT) for the Greenland Blocking Index (GBI). Thick black contours designate the 5% significance levels against red noise and the cone of influence (COI) where edge effects may distort the analysis as shown in a lighter shade. (For interpretation of the references to colour in this figure legend, the reader is referred to the web version of this article.)

Barents Sea has the SST range between −0.01 and 0.05 °C/year, indicating local variations in cooling and warming trends. On similar lines, it should be noted that the Barents Sea shows a warming seasonal trend for the period of 1982–2018; more than 70% of the area shows the high mean warming trends. In winter at 0.035 °C/year whereas other seasons show a trend of 0.014 °C/year (summer trends being 0.008 °C/year). This is interesting, since a theorized increase in ice concentrations (in winter) would naturally lead to a decreasing SST trend. We suggest that the high winter warming trend in the Barents Sea could indicate the ice-cover over this region is relatively low or may be generated within the Nordic Seas. This is theorized due to previous studies indicating a direct influence of warm North Atlantic water masses and ice retreat on the Arctic Ocean SST. Warmer areas around the Barents and Kara Seas (Fig. 4) have been linked to Ural blocking events and consequent sea ice declines in the recent decades (Luo et al., 2016; Luo et al., 2019). Greater losses in sea ice due to increased warming trends as evident in Fig. 6g can also impact climates in the Eurasian continent, thus highlighting major links between Arctic Ocean

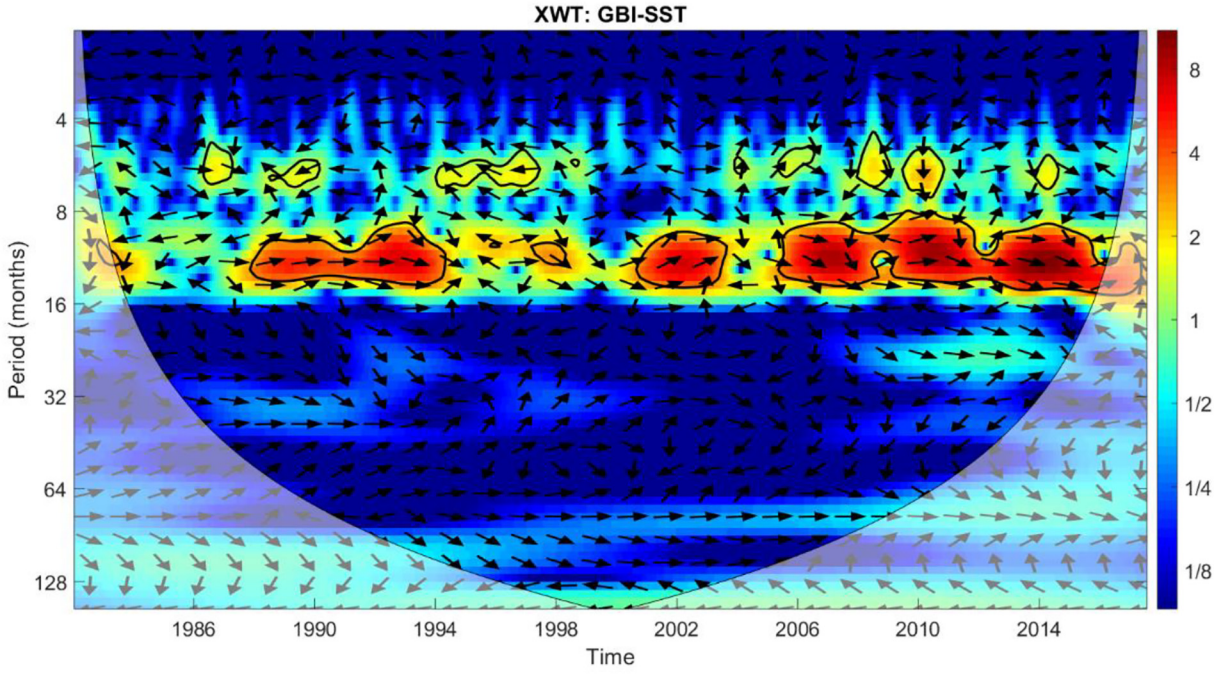

Fig. 9. Cross wavelet transform (XWT) between standardized monthly time series of the Arctic Ocean SST and GBI. The 5% significance level against red noise is shown in thick black contours. Phase relationships are indicated as follows: arrows pointing in the right indicate "in-phase" and arrows pointing to the left indicate "anti-phase" relationships. (For interpretation of the references to colour in this figure legend, the reader is referred to the web version of this article.)

SST and midlatitude cold events. September sea ice concentrations have also declined in the beginning over the past decades (Parkinson and Comiso, 2013). This reduced sea ice could also be contributing to ocean-atmosphere heat fluxes and the subsequent warming of the sea and the atmosphere.

In addition, our findings reveal a unique spatial SST gradient in the autumn trend in the Barents Sea. There is a warming trend off the coasts of Scandinavia and Russia at 0.12 °C/year. As it moves further north towards the coast of Severny Island (Russia), there is a reversal and cooling autumn trend at −0.03 °C/year. Thus, there is a drastic spatial/zonal variation in the autumn trend from the north to south in the Barents Sea. Moreover, the East Siberian and Laptev Seas show a cooling summer trend that can be seen along the Russian coastline (Sakha Republic).

Correlation coefficients were obtained to examine the spatio-temporal correlation between the Arctic Ocean SST and climatic

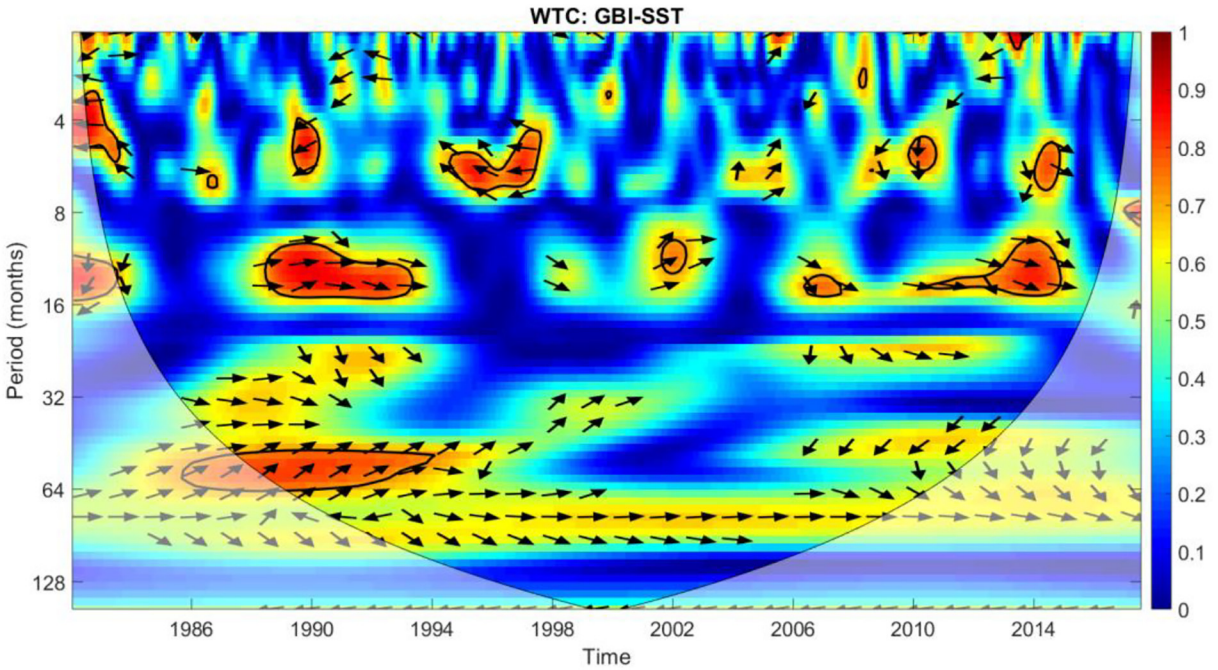

Fig. 10. Wavelet coherence between standardized monthly time series of the Arctic Ocean SST and GBI. Thick contours indicate 5% significance levels against red noise. Most of the insignificant sections show the in-phase behaviour. (For interpretation of the references to colour in this figure legend, the reader is referred to the web version of this article.)

variables. Our findings prove that the Arctic Ocean SST is affected by air temperature ($R = 0.93$), water vapor ($R = 0.88$), wind speed ($R = -0.47$), ozone ($R = -0.39$), total cloud cover ($R = -0.39$) and sea ice concentration ($R = -0.7$). Therefore, positive relationships exist between the Arctic Ocean SST with air temperature and water vapor while a negative (or inverse) relationship exists with sea ice concentration. Notable observations in the spatiotemporal structure of correlations are: i) In comparison to other marginal seas of the Arctic Ocean where positive correlations exist between SST and Ozone ($R = 0.4$–0.5), the Chukchi Sea has a relatively high negative correlation coefficient of -0.8. This emphasizes that ozone is a comprehensive factor in which a decrease in atmospheric ozone can greatly lead to an increase in SST; ii) Despite the overall negative correlation between wind speed and SST ($R = -0.47$), our findings reveal that the Nordic seas (particularly Norwegian and western Barents Sea) have an inverse relationship with wind speed. This implies that wind speed has a considerable effect in enhancing SST in these regions; an increase in wind speed can cause a decrease in local SST and vice versa. Moreover, this inverse relationship between SST with wind speed and ozone (R values between -0.5 and -0.6) can prove as a contributing factor to annual warming trends in the southern and western Barents Sea (Figs. 4, 5c and d). On the contrary, all other seas, particularly the Laptev and East Siberian Seas show a negligible R values, indicating that local SST is not influenced by changes in wind speed.

4.2. Phase relationships between Artic Ocean SST and GBI

This paper serves as a first attempt to examine the relationship between the Arctic Ocean SST and the GBI. The wavelet coherence and cross wavelet analyses were performed on the monthly time series between the Arctic Ocean SST and GBI. Cross wavelet analyses hinted at significant in-phase relationships as represented by “islands” of common power. Nevertheless, it is worth mentioning that cross wavelet spectrums may not be the reliable means to examine phase relationships. A limitation of the XWT is its inability to normalize two time series to a single wavelet spectrum which can be misleading. To improve robustness of our results, therefore, wavelet coherence methods were also used. Our findings indicate that a significant covariance exists between the monthly time series of the Arctic Ocean SST and GBI, particularly for the periods of 1988–1994 and 2012–2014. The GBI shows an increasing seasonal trend since the early 1900s as compared to decreasing or “troughs” from 1880 to late-1980s. Positive winter GBI phases have been recorded in 2010, 2011 and 2013 (Hanna et al., 2016).

Potential vorticity gradients which are known to change due to warming-cooling trends have recently been identified as another climatic factor in affecting Arctic warming. Such gradients have produced regions of tropospheric blocking in Greenland and have been linked with sea ice decline and air temperatures in the Arctic (Luo et al., 2019). Blocking indices in Greenland, can therefore be attributed to changes in Arctic Ocean SST which have also been linked with sea ice loss in the Arctic. Hence, it is possible that seasonal changes in GBI can lead to changes in the Arctic Ocean SST. Furthermore, Greenland blocking anticyclones caused by warming in the high latitude regions of the North Atlantic (Baffin Bay, Davis Strait and Labrador Sea) have been linked to cold anomalies in northern Eurasia (Luo et al., 2016). Increase in SST over these regions (Figs. 2 and 3) can further provoke high pressure blocking regimes in Greenland. Thus further supporting the hypothesis that a relationship is likely to exist between the Arctic Ocean and GBI. These findings are a unique contribution to understanding relationships between the Arctic Ocean SST and regional teleconnection patterns (e.g., GBI). Wavelet analyses prove that a relationship does exist between the Arctic Ocean SST and GBI, which provides a basis for linkages between ocean temperatures and regional climate indices.

5. Summary and conclusions

This paper provides a comprehensive and in-depth analysis of SST variability in the Arctic Ocean and its marginal seas in a changing climate. Various atmospheric variables were examined to reveal correlations with the Arctic Ocean, which provides meaningful insights into the understanding of the potential causes of the SST changes. In addition, the underlying connection between SST and GBI was disclosed through cross wavelet and coherence analysis, which facilitates further studies exploring the complex mechanisms causing extreme weather and climate events as well as teleconnection patterns related to the Arctic Ocean.

In this study, the wavelet analyses were carried out on monthly time series to reveal potential relationships between the Arctic Ocean SST and GBI. A possible caveat can be the timescale/resolution that can affect results i.e. different models (Gaussian etc.) have not been considered in this study. Therefore, future studies would be undertaken to improve the robustness of the wavelet analyses, and to further explore the long-distance teleconnections originating from the Arctic Ocean SST changes.

Declaration of Competing Interest

The authors declare that they have no known competing financial interests or personal relationships that could have appeared to influence the work reported in this paper.

Acknowledgments

This research was supported by the National Natural Science Foundation of China (Grant No. 51809223) and the Hong Kong Polytechnic University Start-up Grant (Grant No. 1-ZE8S). We would like to express our sincere gratitude to the editor and anonymous reviewers for their constructive comments and suggestions.

References

Årthun, M., Eldevik, T., Smedsrud, L.H., 2019. The role of Atlantic heat transport in future Arctic winter sea ice loss. J. Clim. 32, 3327–3341. https://doi.org/10.1175/JCLI-D-18-0750.1.

Carvalho, K.S., Wang, S., 2019. Characterizing the Indian Ocean sea level changes and potential coastal flooding impacts under global warming. J. Hydrol. 569, 373–386. https://doi.org/10.1016/j.jhydrol.2018.11.072.

Chen, H., Wang, S., Wang, Y., 2020. Exploring abrupt alternations between wet and dry conditions on the basis of historical observations and convection-permitting climate model simulations. J. Geophys. Res. Atmos. 125 (9). https://doi.org/10.1029/2019JD031982.

Chepurin, G.A., Carton, J.A., 2012. Subarctic and arctic sea surface temperature and its relation to ocean heat content. J. Geophys. Res. 117, C06019. https://doi.org/10.1029/2011JC007770.

Comiso, J.C., 2003. Warming trends in the Arctic from clear sky satellite observations. J. Clim. 16, 3498–3510. https://doi.org/10.1175/1520-0442(2003)016%3C3498:WTITAF%3E2.0.CO;2.

Dee, D.P., Uppala, S.M., Simmons, A.J., Berrisford, P., Poli, P., Kobayashi, S., Andrae, U., Balmaseda, M.A., Balsamo, G., Bauer, P., Bechtold, P., Beljaars, A.C.M., van de Berg, L., Bidlot, J., Bormann, N., Delsol, C., Dragani, R., Fuentes, M., Geer, A.J., Haimberger, L., Healy, S.B., Hersbach, H., Hólm, E.V., Isaksen, L., Kållberg, P., Köhler, M., Matricardi, M., McNally, A.P., Monge-Sanz, B.M., Morcrette, J.-J., Park, B.-K., Peubey, C., de Rosnay, P., Tavolato, C., Thépaut, J.-N., Vitart, F., 2011. The ERA-Interim reanalysis: configuration and performance of the data assimilation system. Q. J. R. Meteorol. Soc. 137, 553–597. https://doi.org/10.1002/qj.828.

Deser, C., Alexander, M.A., Xie, S.-P., Phillips, A.S., 2010. Sea surface temperature variability: Patterns and mechanisms. Annu. Rev. Mar. Sci. 2, 115–143. https://doi.org/10.1146/annurev-marine-120408-151453.

Deser, C., Phillips, A.S., Alexander, M.A., 2010a. Twentieth century tropical sea surface temperature trends revisited. Geophys. Res. Lett. 37, L10701. https://doi.org/10.1029/2010GL043321.

Fisher, R.A., 1992. Statistical methods for research workers. In: Kotz, S., Johnson, N.L. (Eds.), Breakthrough in Statistics. Springer Series in Statistics (Perspectives in Statistics). Springer, New York. https://doi.org/10.1007/978-1-4612-4380-9_6.

Flatau, M.K., Talley, L., Niiler, P.P., 2003. The North Atlantic Oscillation, Surface Current Velocities, and SST changes in the Subpolar North Atlantic. J. Clim. 16, 2355–2369. https://doi.org/10.1175/2787.1.

Furevik, T., 2000. On Anomalous Sea Surface Temperatures in the Nordic Seas. J. Clim.

13, 1044–1053. https://doi.org/10.1175/1520-0442(2000)013%3C1044:OASSTI%3E2.0.CO;2.
Furevik, T., Mauritzen, C., Ingvaldsen, R., 2007. The flow of Atlantic water to the Nordic Seas and Arctic Ocean. In: Ørbæk, J.B., Kallenborn, R., Tombre, I., Hegseth, E.N., Falk-Petersen, S., Hoel, A.H. (Eds.), Arctic Alpine Ecosystems and People in a Changing Environment. Springer, Berlin, Heidelberg.
Greene, C.A., Thirumalai, K., Kearney, K.A., Delgado, J.M., Schwanghart, W., Wolfenbarger, N.S., et al., 2019. The climate data toolbox for MATLAB. Geochem. Geophys. Geosyst. 20. https://doi.org/10.1029/2019GC008392.
Grinsted, A., Moore, J.C., Jevrejeva, S., 2004. Application of the cross wavelet transform and wavelet coherence to geophysical time series. Nonlinear Process. Geophys. 11, 561–566. https://doi.org/10.5194/npg-11-561-2004.
Hanna, E., Cropper, T.E., Hall, R.J., Cappelen, J., 2016. Greenland Blocking Index 1851-2015: a regional climate change signal. Int. J. Climatol. 36, 4847–4861. https://doi.org/10.1002/joc.4673.
Holland, M.M., Bitz, C.M., 2003. Polar amplification of climate change in coupled models. Clim. Dyn. 21, 221–232. https://doi.org/10.1007/s00382-003-0332-6.
Hurrell, J.W., 1995. Decadal trends in the North Atlantic Oscillation: Regional temperatures and Precipitation. Science 269 (5224), 676–679. https://doi.org/10.1126/science.269.5224.676.
IPCC, 2014. In: Barros, V.R. (Ed.), Climate Change 2014: Impacts, Adaptation, and Vulnerability. Part B: Regional Aspects. Contribution of Working Group II to the Fifth Assessment Report of the Intergovernmental Panel on Climate Change. Cambridge University Press, Cambridge, United Kingdom and New York, NY, USA, pp. 1655–1731.
Jakowczyk, M., Stramska, M., 2014. Spatial and temporal variability of satellite-derived sea surface temperature in the Barents Sea. Int. J. Remote Sens. 35 (17), 6545–6560. https://doi.org/10.1080/01431161.2014.958247.
Lee, S., Gong, T., Feldstein, S.B., Screen, J.A., Simmonds, I., 2017. Revisiting the cause of the 1989-2009 Arctic surface warming using the surface energy budget: Downward infrared radiation dominates the surface fluxes. Geophys. Res. Lett. 44, 10654–10661. https://doi.org/10.1002/2017GL075375.
Luo, B., Wu, L., Luo, D., Dai, A., Simmonds, I., 2019. The winter midlatitude-Arctic interaction: Effects of North Atlantic SST and high-latitude blocking on Arctic sea ice and Eurasian cooling. Clim. Dyn. 52, 2981–3004. https://doi.org/10.1007/s00382-018-4301-5.
Luo, D., Xiao, Y., Yao, Y., Dai, A., Simmonds, I., Franzke, C.L.E., 2016. Impact of Ural blocking on winter warm Arctic–cold Eurasian anomalies. Part I: Blocking-induced amplification. J. Clim. 29, 3925–3947. https://doi.org/10.1175/JCLI-D-15-0611.1.
Luo, D., Chen, X., Overland, J., Simmonds, I., Wu, Y., Zhang, P., 2019. Weakened potential vorticity barrier linked to recent winter Arctic sea ice loss and midlatitude cold extremes. J. Clim. 32, 4235–4261. https://doi.org/10.1175/JCLI-D-18-0449.1.
Luo, B., Luo, D., Wu, L., Zhong, L., Simmonds, I., 2017. Atmospheric circulation patterns which promote winter Arctic sea ice decline. Environ. Res. Lett. 12, 054017. https://doi.org/10.1088/1748-9326/aa69d0.
Manabe, S., Stouffer, R.J., 1980. Sensitivity of a global climate model to an increase of CO_2 concentration in the atmosphere. J. Geophys. Res. Oceans 85, 5529–5554. https://doi.org/10.1029/JC085iC10p05529.
Miller, G.H., Alley, R.B., Brigham-Grette, J., Fitzpatrick, J.J., Polyak, L., Serreze, M.C., White, J.W.C., 2010. Arctic amplification: can the past constrain the future? Quat. Sci. Rev. 29 (15–16), 1779–1790. https://doi.org/10.1016/j.quascirev.2010.02.008.
Overland, J., Dunlea, E., Box, J.E., Corell, R., Forsius, M., Kattsov, V., Olsen, M.S., Pawlak, J., Reiersen, L., Wang, M., 2019. The urgency of Arctic change. Polar Sci. 21, 6–13. https://doi.org/10.1016/j.polar.2018.11.008.
Parkinson, C.L., Comiso, J.C., 2013. On the 2012 record low Arctic sea ice cover: Combined impact of preconditioning and an August storm. Geophys. Res. Lett. 40, 1356–1361. https://doi.org/10.1002/grl.50349.
Pavlova, O., Pavlov, V., Gerland, S., 2014. The impact of winds and sea surface temperatures on the Barents Sea ice extent, a statistical approach. J. Mar. Syst. 130, 248–255. https://doi.org/10.1016/j.jmarsys.2013.02.011.
Reynolds, R.W., Marsico, D.C., 1993. An improved real-time global sea surface temperature analysis. J. Clim. 6, 114–119. https://doi.org/10.1175/1520-0442(1993)006%3C0114:AIRTGS%3E2.0.CO;2.
Reynolds, R.W., Smith, T.M., Liu, C., Chelton, D.B., Casey, K.S., Schlax, M.G., 2007. Daily high-resolution-blended analyses for sea surface temperature. J. Clim. 20, 5473–5496. https://doi.org/10.1175/2007JCLI1824.1.
Screen, J.A., Bracegirdle, T.J., Simmonds, I., 2018. Polar climate change as manifest in atmospheric circulation. Curr. Clim. Chang. Rep. 4, 383–395. https://doi.org/10.1007/s40641-018-0111-4.
Serreze, M.C., Barry, R.G., 2011. Processes and impacts of Arctic amplification: A research synthesis. Glob. Planet. Chang. 77 (1–2), 85–96. https://doi.org/10.1016/j.gloplacha.2011.03.004.
Serreze, M.C., Barrett, A.P., Stroeve, J.C., Kindig, D.N., Holland, M.M., 2009. The emergence of surface-based Arctic amplification. Cryosphere 3, 11–19. https://doi.org/10.5194/tc-3-11-2009.
Simmonds, I., 2015. Comparing and contrasting the behaviour of Arctic and Antarctic sea ice over the 35-year period 1979-2013. Ann. Glaciol. 56 (69), 18–28. https://doi.org/10.3189/2015AoG69A909.
Steele, M., Dickinson, S., 2016. The phenology of Arctic Ocean surface warming. J. Geophys. Res. Oceans 121, 6847–6861. https://doi.org/10.1002/2016JC012089.
Stroh, J.N., Panteleev, G., Kirrilov, S., Makhotin, M., Shakova, N., 2015. Sea-surface temperature and salinity product comparison against external in situ data in the Arctic Ocean. J. Geophys. Res. Oceans 120, 7223–7236. https://doi.org/10.1002/2015JC011005.
Tang, Y., 2012. The effect of variable sea surface temperature on forecasting sea fog and sea breezes: A case Study. J. Appl. Meteorol. Climatol. 51 (5), 986–990. https://doi.org/10.1175/JAMC-D-11-0253.1.
Torrence, C., Compo, G.P., 1998. A practical guide to wavelet analysis. Bull. Amer. Meteor. Soc. 79, 61–78. https://doi.org/10.1175/1520-0477(1998)079%3C0061:APGTWA%3E2.0.CO;2.
Torrence, C., Webster, P., 1999. Interdecadal changes in the ENSO-monsoon system. J. Clim. 12, 2679–2690. https://doi.org/10.1175/1520-0442(1999)012%3C2679:ICITEM%3E2.0.CO;2.
Wang, S., Wang, Y., 2019. Improving probabilistic hydroclimatic projections through high-resolution convection-permitting climate modeling and Markov chain Monte Carlo simulations. Clim. Dyn. 53, 1613–1636. https://doi.org/10.1007/s00382-019-04702-7.
Wang, S., Ancell, B., Huang, G., Baetz, B., 2018. Improving robustness of hydrologic ensemble predictions through probabilistic pre- and post-processing in sequential data assimilation. Water Resour. Res. 54 (3), 2129–2151. https://doi.org/10.1002/2018WR022546.
Wang, Q., Wang, X., Wekerle, C., Danilov, S., Jung, T., Koldunov, N., Lind, S., Sein, D., Shu, Q., Sidorenko, D., 2019. Ocean heat transport into the Barents Sea: Distinct controls on the upward trend and interannual variability. Geophys. Res. Lett. 46, 13180–13190. https://doi.org/10.1029/2019GL083837.
Yao, Y., Luo, D., Dai, A., Simmonds, I., 2017. Increased quasi stationarity and persistence of winter Ural blocking and Eurasian extreme cold events in response to Arctic warming. Part I: Insights from Observational Analyses. J. Clim. 30, 3549–3568. https://doi.org/10.1175/JCLI-D-16-0261.1.
Yeo, S., Kim, K., Yeh, S., Kim, B., Shim, T., Jhun, J., 2014. Recent climate variation in the Bering and Chukchi Seas and its linkages to large-scale circulation in the Pacific. Clim. Dyn. 42, 2423–2437. https://doi.org/10.1007/s00382-013-2042-z.
Zanna, L., Khatiwala, S., Gregory, J., Ison, J., Heimbach, P., 2019. Global reconstruction of historical ocean heat storage and transport. Proc. Natl. Acad. Sci. U. S. A. 116 (4), 1126–1131. https://doi.org/10.1073/pnas.1808838115.
Zar, J.H., 1999. Biostatistical Analysis. Prentice Hall, New Jersey.
Zhang, B., Wang, S., Wang, Y., 2019. Copula-based convection-permitting projections of future changes in multivariate drought characteristics. J. Geophys. Res. Atmos. 124 (14), 7460–7483. https://doi.org/10.1029/2019JD030686.